

Mode-I stress intensity factor in single layer graphene sheets



Minh-Quy Le^a, Romesh C. Batra^{b,*}

^a Department of Mechanics of Materials and Structures, School of Mechanical Engineering, Hanoi University of Science and Technology, No. 1, Dai Co Viet Road, Hanoi, Viet Nam

^b Department of Biomedical Engineering and Mechanics, M/C 0219, Virginia Polytechnic Institute and State University, Blacksburg, VA 24061, USA

ARTICLE INFO

Article history:

Received 17 January 2016

Received in revised form 10 March 2016

Accepted 18 March 2016

Available online 31 March 2016

Keywords:

Crack propagation

Graphene

Molecular dynamics

Stress intensity factor

ABSTRACT

We use the freely available software, LAMMPS, and the Tersoff potential to find the mode-I stress intensity factor during crack propagation in an edge-cracked single layer graphene sheet deformed at a constant axial strain rate. The axial stress and the stress intensity factor (SIF) at atoms' locations are computed by using, respectively, the Virial theorem and either the stress at the atom located at the crack-tip or the average axial stress in the sheet. It is found that the two values of the SIF differ from each other by about 8%, and agree with those reported in the literature derived either analytically or from test data. The method proposed and used herein can be applied to find the SIF in any nanostructure.

© 2016 Elsevier B.V. All rights reserved.

1. Introduction

Single layer graphene sheets (SLGSs) and nano-composites with graphene sheets as reinforcements have generally superior specific mechanical [1], thermal [2], and electronic [3] properties than many other monolithic and composite materials, and have potential applications in nano-electronic devices [4,5]. Needless to say, the fracture of SLGSs plays a significant role in designing graphene-based materials and structures. One parameter used to determine the fracture of a SLGS is the stress intensity factor (SIF).

Several continuum fracture mechanics concepts in conjunction with atomistic simulations have been explored to investigate fracture of graphene sheets. Some authors [6–8] have used the definition of the energy release rate, i.e., the negative of the derivative of the potential energy with respect to the crack surface area, to find fracture toughness of a graphene sheet using results of molecular dynamics (MD) simulations. Xu et al. [9] have used the crack-tip displacement field and a coupled quantum mechanics (QM)/continuum mechanics analysis and reported values, 3.71 and 4.21 MPa√m, of the SIF in the armchair and the zigzag directions, respectively. The well-known relation, Eq. (1), between the critical SIF, the fracture stress, and the initial crack length has been used to interpret fracture toughness tests [10,11] of polycrystalline graphene and in theoretically predicting the SIF in single layer crystalline graphene [12]:

$$K_{Ic} = \sigma_f \sqrt{\pi a_0}. \quad (1)$$

Here K_{Ic} , σ_f and a_0 are, respectively, the critical mode-I SIF, the fracture stress, and the half initial crack length of a centered crack. Nakatani et al. [13] proposed an atomic version of the J -integral, that has been applied to study fracture of graphene sheets [14,15].

Most of the above-cited approaches are limited to predicting the critical SIF at failure (fracture toughness) of graphene and do not allow the evaluation of the SIF for a propagating crack. It should be noted that Nakatani et al.'s [13] atomic version of the J -integral could be used in principle to compute the SIF during crack propagation. However, its implementation is complicated and the method is difficult to use for branching cracks. Recently, using the definition of the J -integral, Le and Batra [16,17] evaluated its value for SLGSs deformed in simple tension. However, this method seems ambiguous for propagating cracks because during crack propagation not only a broken bond that updates the crack length but also the internal relaxation affect the potential energy of a SLGS.

Evaluations of the SIF during crack propagation in nanostructures such as a SLGS, a polycrystalline graphene, and other nano-materials is still an open issue. The determination of the SIF for a crack propagating in a nanostructure is challenging due to the discreteness of the atomic system and crack branching. Here we propose a simple method based on the crack-tip stress field to compute the SIF during the entire fracture process. In principle, this method can be applied to any nanostructure. However, numerical results are only provided here for a SLGS with cracks propagating from one edge in either the armchair or the zigzag direction. Effects of the initial crack length and three values of the average axial strain rate on the SIF value have been delineated.

* Corresponding author. Tel.: +1 540 231 6051; fax: +1 540 231 4574.

E-mail address: rbatra@vt.edu (R.C. Batra).

2. Computational setup

2.1. Interatomic potentials

The potential energy, E , in the Tersoff potential used to model the interatomic interactions [18] is given by

$$E = \sum_i E_i = \frac{1}{2} \sum_{i,j,i \neq j} V_{ij}, \quad V_{ij} = f_C(r_{ij}) [f_R(r_{ij}) + b_{ij} f_A(r_{ij})]; \quad (2a)$$

$$f_R(r_{ij}) = A_{ij} \exp(-\lambda_{ij}^I r_{ij}), \quad f_A(r_{ij}) = -B_{ij} \exp(-\lambda_{ij}^{II} r_{ij}); \quad (2b)$$

$$f_C(r_{ij}) = \begin{cases} 1, & r_{ij} \leq R_{ij}; \\ \frac{1}{2} + \frac{1}{2} \cos\left(\pi \frac{r_{ij} - R_{ij}}{S_{ij} - R_{ij}}\right), & R_{ij} \leq r_{ij} \leq S_{ij}; \\ 0, & r_{ij} \geq S_{ij}; \end{cases} \quad (2c)$$

$$b_{ij} = \chi_{ij} (1 + \beta_i^{n_i} \zeta_{ij}^{n_i})^{-1/2n_i}, \quad \zeta_{ij} = \sum_{k \neq i,j} f_C(r_{ik}) \omega_{ik} g(\theta_{ijk}), \\ g(\theta_{ijk}) = 1 + c_i^2/d_i^2 - c_i^2/[d_i^2 + (h_i - \cos \theta_{ijk})^2] \quad (2d)$$

The lower case Latin indices i, j and k are labels for atoms in the system. The three indices i, j and k on a symbol imply that the interaction between atoms i and j is modified by the atom k . r_{ij} is the distance between atoms i and j , f_A and f_R are the attractive and the repulsive pairwise terms, f_C is a cutoff function to ensure the nearest-neighbor interactions and economize on the computational cost, R_{ij} and S_{ij} denote, respectively, the small and the large cutoff distances, and b_{ij} is a bond-order parameter that depends on local coordinates of atoms around atom i . Values of the force field parameters in Eq. (2), taken from [18,19] for C–C interactions, are listed in Table 1.

2.2. Cutoff function

It is well known that the overestimation of the maximum force needed to break an interatomic bond is caused by the cutoff function, Eq. (2c), e.g., see [20]. Consequently, it leads to overestimation of stresses and strains in atomic structures simulated with the Tersoff–Brenner [20–22] and the REBO [23] potentials. In order to avoid this, many authors have used the small cutoff distance given by $R_{ij} = S_{ij}$, e.g., see [22–25]. It should be noted that when the small cutoff distance is extended to the large one, the cutoff function allows, before failure, bond strains of about 46% and 44% for C–C interactions with the Tersoff [18] and the REBO potentials [26], respectively. Belytschko et al. [20] have reported that the cutoff function affects the fracture behavior even when bond strains of 100% are considered.

In the present study, the cut-off function is not considered. Instead, as suggested by Shenderova et al. [21] and later adopted by several authors [14,27,28], a bond list is created for the initial system and used during the entire simulation.

2.3. Molecular dynamics (MD) simulations

MD simulations were carried out using the freely available software LAMMPS [29] in a micro-canonical (NVE) ensemble with the temperature kept at 0.001 K using the Langevin dynamics [30].

Periodic boundary conditions are used in the direction of tensile loading, and these atoms are restrained from moving in the lateral direction. Atoms on the specimen edges parallel to the tensile direction are free, i.e., no external force is applied on them. After relaxation for 50 ps (pico-seconds), the specimen was deformed in the armchair and the zigzag directions as indicated in Fig. 1 by applying a constant strain rate in the tensile direction. Most simulations were carried out at an axial strain rate of $2.5 \times 10^8 \text{ s}^{-1}$ with additional simulations at axial strain rates of $2.5 \times 10^7 \text{ s}^{-1}$ and $2.5 \times 10^6 \text{ s}^{-1}$.

Pristine SLGSs of 58,880 atoms when relaxed at 0.001 K had C–C bond length of 1.44 Å with $\sim 397.1 \text{ Å}$ ($\sim 397.4 \text{ Å}$) length in the zigzag (armchair) direction. A single edge pre-crack initially perpendicular to the tensile loading direction is created by removing a group of atoms as schematically illustrated in Fig. 1.

The strain energy, U , due to deformation of the structure is determined by subtracting the energy of the relaxed structure (the energy at zero strain) from that of the loaded structure (the energy at a given strain). The conventional axial stress (average axial stress in the sheet), σ , and Young's modulus, Y , of the sheet are defined as

$$\sigma = \frac{1}{V_0} \frac{\partial U}{\partial \varepsilon}, \quad Y = \frac{1}{V_0} \left. \frac{\partial^2 U}{\partial \varepsilon^2} \right|_{\varepsilon=0}, \quad (3)$$

where V_0 is the initial volume of the structure. Note that $V_0 = S_0 t$, where S_0 is the initial surface area of the structure and t the sheet's thickness. The 2D stress, σ_{2D} , and the 2D Young's modulus (or the in-plane stiffness), Y_s , defined below are computed.

$$\sigma_{2D} = \sigma t = \frac{1}{S_0} \frac{\partial U}{\partial \varepsilon}, \quad Y_s = Y t = \frac{1}{S_0} \left. \frac{\partial^2 U}{\partial \varepsilon^2} \right|_{\varepsilon=0}. \quad (4)$$

Here, we set $t = 3.4 \text{ Å}$ for comparing our results with those available in the literature. We note that Gupta and Batra [31] studied vibrations of free single layer zigzag and armchair graphene sheets by using molecular mechanics simulations with the MM3 potential, equated frequencies so found with those of a continuous structure of the same size as the graphene sheet and found t varying between 0.82 and 1.0 Å. Using different techniques other authors had found t between 0.618 and 3.4 Å. For example, for a single wall carbon nanotube usually considered to be formed by rolling a SLGS, Batra and Gupta [32] found the wall thickness to be 1 Å.

The Virial theorem [33,34] gives the following expression for the atomic stress tensor.

$$\boldsymbol{\sigma}^{(a)} = \frac{1}{V^{(a)}} \left[-m^{(a)} \mathbf{v}^{(a)} \otimes \mathbf{v}^{(a)} + \frac{1}{2} \sum_{a \neq b} \mathbf{r}^{(ab)} \otimes \mathbf{f}^{(ab)} \right]. \quad (5)$$

In Eq. (5) $V^{(a)}$ is the volume occupied by atom a , $m^{(a)}$ and $\mathbf{v}^{(a)}$ are, respectively, the mass and the velocity vector of atom a , the symbol \otimes denotes the tensor product between two vectors, $\mathbf{r}^{(a)}$ denotes the position vector of atom a , $\mathbf{r}^{(ab)} = \mathbf{r}^{(b)} - \mathbf{r}^{(a)}$ is the position vector of atom b relative to that of atom a , and $\mathbf{f}^{(ab)}$ is the interatomic force exerted on atom a by atom b , where $\mathbf{f}^{(ab)} = \frac{\partial E}{\partial \mathbf{r}^{(ab)}} = \frac{\partial E}{\partial \mathbf{r}^{(ab)}} \frac{\mathbf{r}^{(ab)}}{r^{(ab)}}$, E is the energy of the atomic ensemble and is given by Eq. (2). For a SLGS, $V^{(a)} = S^{(a)} t$, where $S^{(a)}$ is the surface area occupied by atom a .

Table 1
Parameters of the Tersoff potential for C–C interaction [18,19].

A (eV)	B (eV)	$\lambda^I (\text{Å}^{-1})$	$\lambda^{II} (\text{Å}^{-1})$	n	β	c	d	h
1393.6	430.0	3.4879	2.2119	0.72751	1.5724E-7	38,049	4.3484	-0.93

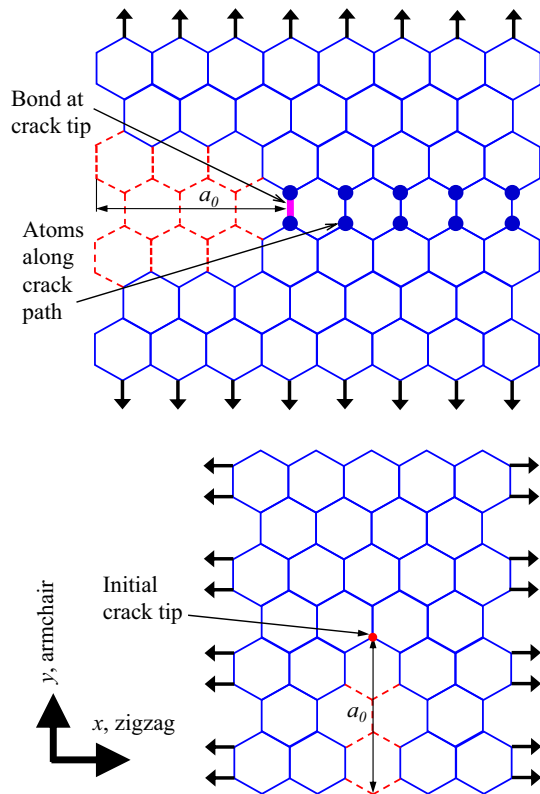


Fig. 1. Schematic illustration of a single edge pre-crack (top) in an armchair graphene sheet under uniaxial tension in the armchair direction, and (bottom) in a zigzag graphene sheet under uniaxial tension in the zigzag direction. Initial crack is created by removing atoms.

3. General considerations

The evolution with the axial strain of the strain energy per unit surface area, namely the surface strain energy density, and the axial stress is plotted in Fig. 2 for the pristine SLGS. Mechanical properties of the pristine graphene sheet derived from our MD simulations and listed in Table 2 agree well with those from previous DFT calculations [35,36] and with that found from test data [1].

In Fig. 3 we have exhibited the axial stress distribution around the crack tip in pre-cracked SLGSs deformed in uniaxial tension in the armchair and the zigzag directions. It is found from results plotted in Figs. 3–5 that the peak stress occurs at the crack-tip. Behind the crack-tip, the stress drops, the stress rapidly decreases ahead of the crack-tip, and is essentially constant relatively far (>3 times the crack length) from the crack-tip. We note that irrespective of the initial crack length the atom with the highest tensile axial stress is the crack-tip, and the axial stress at an atom bonded to the one at the crack-tip reaches the peak value when the bond strain equals about 106–110% and 119–123% in the armchair and the zigzag directions, respectively. Hence, when the axial stress at an atom bonded to the atom at the crack-tip reaches its peak value the bond is broken and the crack is elongated. This criterion is equivalent to using the bond strain of about 100% for breaking the bond as was assumed in our earlier work [16,17].

As should be clear from the results exhibited in Fig. 5 the location of the crack-tip shifts from one atom to another atom as the crack propagates. The evolution of the tensile axial stress at the first and the second atoms along the crack path versus the bond strain at the initial crack-tip is shown in Fig. 4 for the two pre-cracked graphene sheets. This bond contains the first atom (or the initial crack-tip) and the adjoining atom where the axial

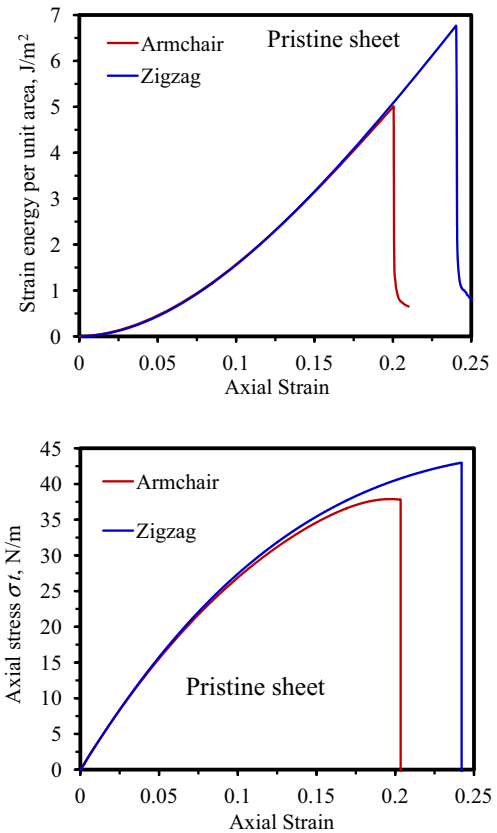


Fig. 2. Evolution of (top) strain energy per unit surface area and (bottom) axial stress versus axial strain for the pristine graphene sheet under uniaxial tension in the armchair and the zigzag directions.

Table 2

Mechanical properties of pristine graphene sheets.

Reference	In-plane stiffness Y_s (N/m)	Maximum in-plane stress (N/m)	Axial strain at the maximum stress (%)
Present study	358 (zigzag) 350 (armchair)	43.0 (zigzag) 37.9 (armchair)	24 (zigzag) 19.3 (armchair)
DFT (Liu et al. [35])	351	40.4 (zigzag) 36.7 (armchair)	26.6 (zigzag) 19.4 (armchair)
Hyperelastic model & DFT (Xu et al. [36])	350	40.0 (zigzag) 36.4 (armchair)	24 (zigzag) 19 (armchair)
Experiments (Lee et al. [1])	340 ± 50	42 ± 4	25%

tensile stress reaches its peak value next. It is clear that the atomic stress at the initial crack-tip reaches its peak value when the axial strain in the bond equals about 21–22% and 20–21% for tensile loading in the armchair and the zigzag directions, respectively, is nearly independent of the initial crack length, and the maximum difference in its peak values is less than 3% for a wide range of initial crack lengths considered here. The axial tensile stress at the adjoining atom in the crack path slightly depends on the initial crack length. In Fig. 6 we have plotted the evolution of the conventional axial stress in the sheet and the atomic stress for the atom at the initial crack-tip. The average axial stress in the sheet and the Virial stress at the atom located at the initial crack-tip reach their maximum values at about the same values of the axial strain.

For each strain rate, with monotonically increasing load the crack propagates straight ahead in the armchair direction as shown

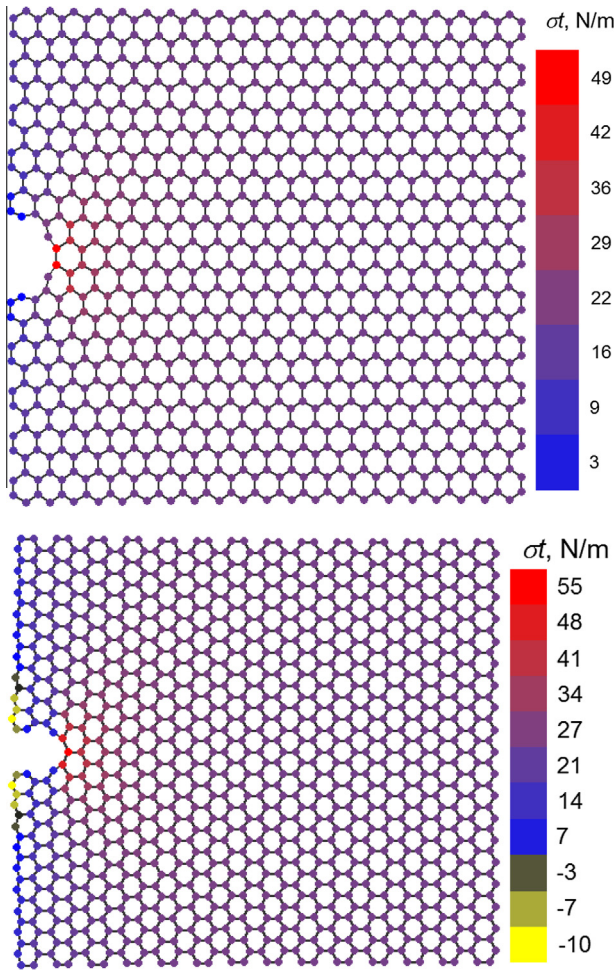


Fig. 3. Axial stresses at atoms around the initial crack-tip just before the crack begins to propagate in the graphene sheet at axial strain (top) $\varepsilon = 7.75525\%$, $a_0 = 3.5d$ ($a_0/w = 0.022$) under tension in the armchair direction, (bottom) $\varepsilon = 8.4455\%$, $a_0 = 5r$ ($a_0/w = 0.018$), under tension in the zigzag direction, r is the bond length, d is the lattice constant and w is the sheet width.

in Fig. 7, and the crack path in the armchair SLGSs is independent of the nominal strain rate. However, under tensile stress in the zigzag direction, the crack kinks and branches as clearly seen in plots of Fig. 8, and the fracture pattern weakly depends on the strain rate. In the problem for which results are shown in Fig. 8, the number of broken bonds equal 208, 211, 210 for strain rates of $2.5 \times 10^6 \text{ s}^{-1}$, $2.5 \times 10^7 \text{ s}^{-1}$ and $2.5 \times 10^8 \text{ s}^{-1}$, respectively. While the number of broken bonds is virtually the same for the three strain rates, the fracture patterns for strain rates of $2.5 \times 10^7 \text{ s}^{-1}$ and $2.5 \times 10^8 \text{ s}^{-1}$ are different, but those for strain rates of $2.5 \times 10^6 \text{ s}^{-1}$ and $2.5 \times 10^7 \text{ s}^{-1}$ are almost identical to each other. The fractured shape of this sheet for the strain rate of $2.5 \times 10^6 \text{ s}^{-1}$ is not shown in Fig. 8 due to its similarity with that for the strain rate of $2.5 \times 10^7 \text{ s}^{-1}$.

4. Stress intensity factor

4.1. Methods

In linear elastic fracture mechanics (LEFM), the mode-I SIF is defined by Eq. (6) [37]:

$$K_I = \frac{1}{f(\theta)} \lim_{\rho \rightarrow 0} \sigma_{YY} \sqrt{2\pi\rho}, \quad (6)$$

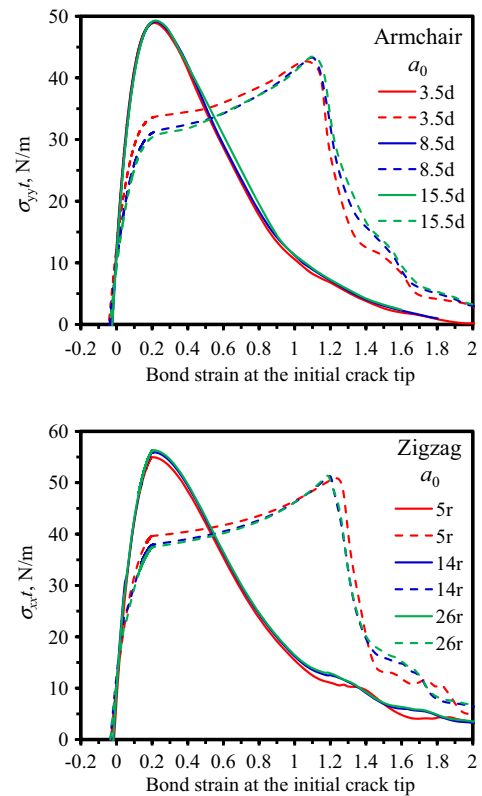


Fig. 4. Evolution of the tensile axial stress at the first (solid curve) and the second (dashed curve) atoms along the crack path versus the bond strain at the initial crack tip (this bond has the first atom and is first broken) in single layer graphene sheets with a single edge pre-crack under uniaxial tension in the (top) armchair and (bottom) the zigzag directions.

$$f(\theta) = \cos\left(\frac{\theta}{2}\right) \left[1 + \sin\left(\frac{\theta}{2}\right) \sin\left(\frac{3\theta}{2}\right) \right]. \quad (7)$$

In Eqs. (6) and (7), (X, Y) is a local coordinate system with origin at the crack-tip, e.g., see Fig. 9 and the Y -axis is along the tensile direction (the x and y -direction, respectively, for tension in the zigzag and the armchair direction), (ρ, θ) are polar coordinates of a point with origin at the crack-tip with the angle θ measured counter-clockwise from the X -axis.

In contrast to the stress state at a crack-tip in a linear elastic continuous body, the atomic stress at a crack-tip in the graphene sheet being studied does not tend to infinity. Stresses at the crack-tip stay finite as the crack propagates through the sheet as shown in Figs. 3–5. Thus, Eq. (6) cannot be applied directly to atoms in the graphene sheet, and we propose the following approximation of Eq. (6) for estimating the SIF.

$$K_I \approx \frac{1}{f(\theta)} \sigma_{YY}^* \sqrt{2\pi\rho^*}. \quad (8)$$

To use Eq. (8), we focus on 2 atoms. The first one is the actual crack-tip identified as the atom in the crack path with the highest axial stress amongst all neighboring atoms around it. The second atom is the next atom in the crack path that will subsequently become the crack-tip and its associated bond will break in subsequent tensile loading. The tensile stress σ_{YY}^* is for this second atom, and ρ^* is the distance between these two atoms. This method allows us to compute the SIF as a crack propagates in the graphene sheet.

It should be emphasized that during monotonic loading, the stresses at atoms along the crack path monotonically increase, reach their maximum values, and then decrease as clearly seen

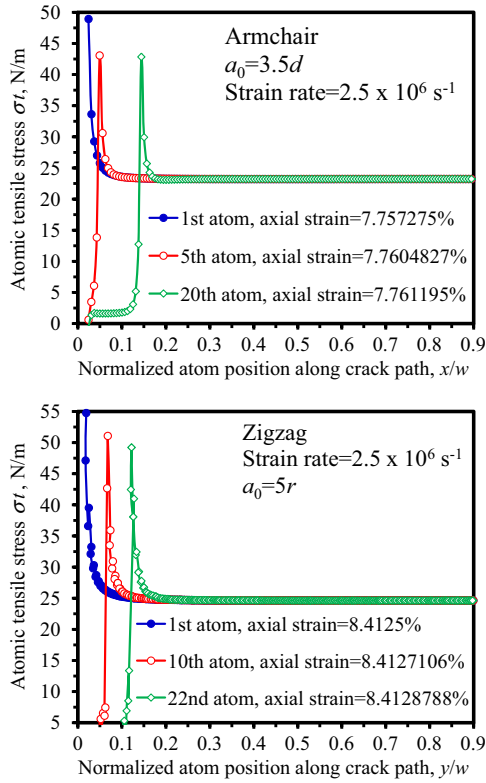


Fig. 5. Axial stress at atoms along the crack path at different stages during crack propagation in the single layer graphene sheet with a single edge crack under uniaxial tension in (top) armchair direction, $a_0 = 3.5d$ ($a_0/w = 0.022$), and (bottom) zigzag direction, $a_0 = 5r$ ($a_0/w = 0.018$). The peak stress at each stage corresponds to the actual crack-tip position. The axial strain when the axial stress at the crack-tip equals its maximum value is indicated in the figure.

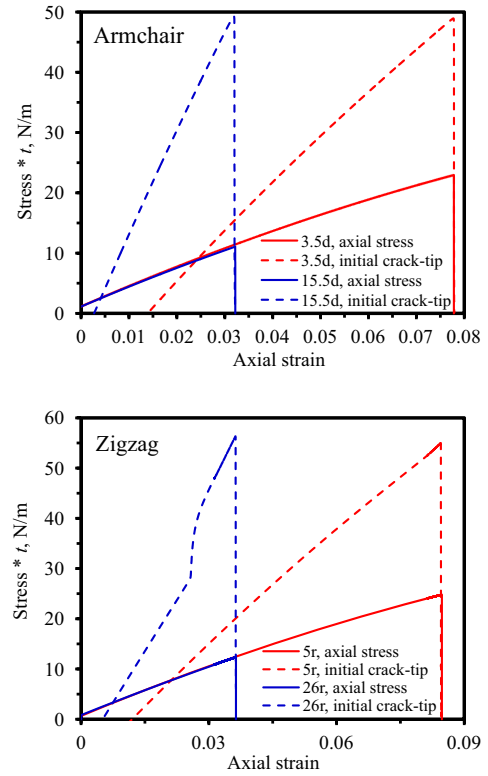


Fig. 6. Evolution of the average axial stress in the sheet and the atomic stress at the initial crack-tip in a single layer graphene sheet with a single edge crack under uniaxial tension in (top) armchair ($a_0 = 3.5d$ and $15.5d$), and (bottom) zigzag ($a_0 = 5r$ and $26r$) directions.

in the plots of Figs. 4 and 5. The decrease in the atomic stress is due to the elongation of the bond associated with the atom at the crack-tip. Graphene exhibits brittle fracture with rapid fracture propagation and a drop in the axial stress–axial strain curve as found in our previous works [16,17] and clearly seen in results displayed in Fig. 6. The conventional axial stress in the sheet and the atomic stress of the initial crack-tip reach their maximum values approximately at the same axial strain as indicated in Fig. 6. Therefore, the critical value of the SIF is estimated when the axial stress at the atom located at the *initial* crack-tip reaches its maximum value. Just beyond this point, the average axial stress in the sheet reaches its maximum value, and the local rupture and the subsequent drop in the load supported by the sheet occur.

The SIF can also be estimated from the following LEFM equation [37] instead of Eq. (6):

$$K_I = 1.12\sigma\sqrt{\pi a_0}, \quad (9)$$

where a_0 is the initial crack length, and σ the average axial stress in the sheet.

4.2. SIF results

The evolution of the SIF versus the average axial tensile stress before the crack begins to propagate is plotted in Fig. 10 with the final point in each curve corresponding to the critical SIF. It should be emphasized that K_{Ic} from Eq. (8) with the crack-tip stress field is computed when the axial stress at the atom located at the initial crack-tip reaches its maximum value, while K_{Ic} from Eq. (9) which uses the global stress is calculated at the maximum value of the average stress in the sheet. The difference in the axial tensile

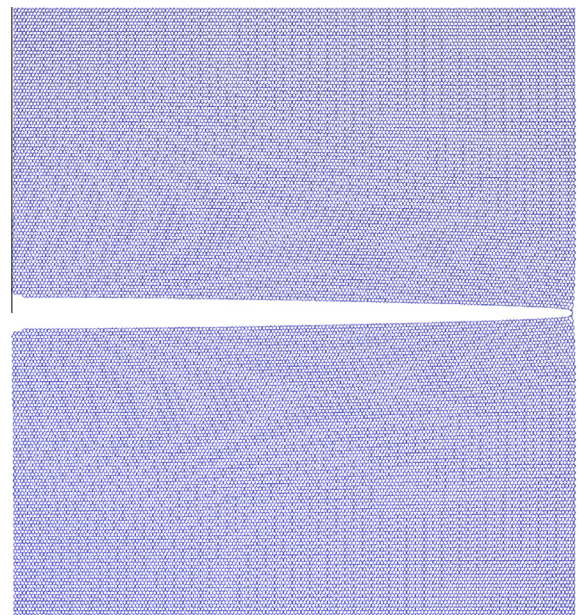


Fig. 7. Fracture of a single layer graphene sheet with a single edge pre-crack of length $a_0 = 3.5d$ ($a_0/w = 0.022$) under uniaxial tension in the armchair direction (the vertical direction in this figure). The fracture pattern is independent of the strain rate.

strains corresponding to these two points is very small, of the order of 0.001%. According to Eq. (9), the SIF increases linearly with an increase in the average axial stress. For tensile loading in the armchair direction, the SIF computed from Eq. (8) also increases

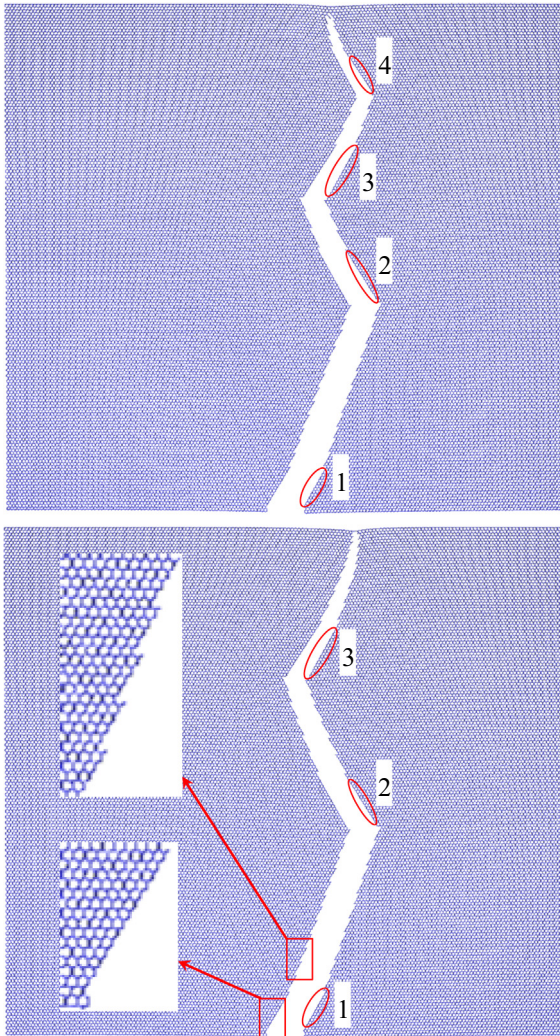


Fig. 8. Crack kinks and branches in a zigzag graphene sheet with a single edge pre-crack of length $a_0 = 5r$ ($a_0/w = 0.018$) under tension in the zigzag direction (the horizontal direction in this figure). (top) Strain rate = $2.5 \times 10^8 \text{ s}^{-1}$, and (bottom) strain rate = $2.5 \times 10^7 \text{ s}^{-1}$. Red ellipses indicate smooth shapes of crack face; see also Fig. 12 and the text for details. (For interpretation of the references to color in this figure legend, the reader is referred to the web version of this article.)

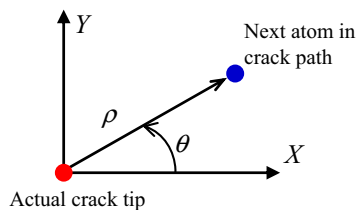


Fig. 9. Schematic illustration of an atom at the crack tip and the next atom in the crack path. The vector passing through these two atoms shows the distance ρ in polar coordinates. These two atoms are never in the same bond. Y is the tensile direction (the x and y -direction for tension in the zigzag and armchair directions, respectively).

linearly with an increase in the axial stress. However, for tensile loading in the zigzag direction, the SIF computed using Eq. (8) increases linearly with increasing axial stress for relatively small initial crack lengths (small value of a_0/w), but for large initial crack lengths, it first increases linearly and then approaches the curve computed using Eq. (9). This is due to the way the atomic stress is computed and displacements of atoms along the crack path.

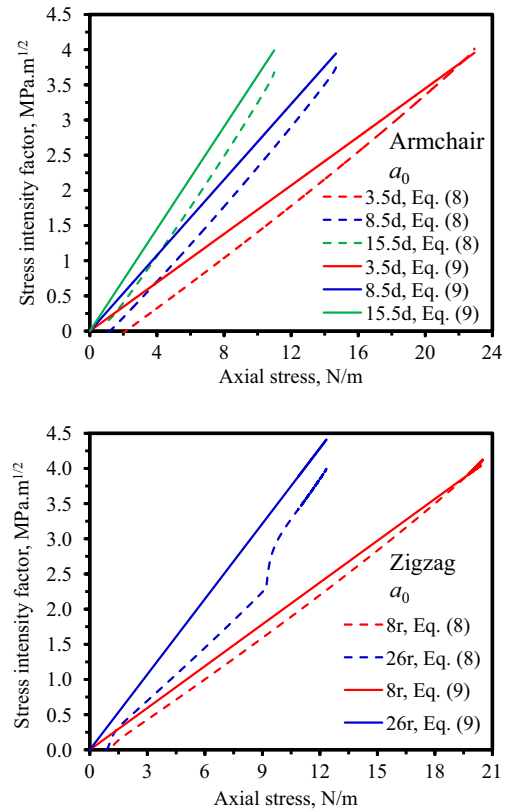


Fig. 10. Evolution of the stress intensity factor K_I versus the axial tensile stress before crack propagation in single layer graphene sheets with a single edge pre-crack, (top) under uniaxial tension in the armchair direction, and (bottom) under uniaxial tension in the zigzag direction. The final point in each curve corresponds to the critical stress intensity factor K_{Ic} .

The following three factors affect the evolution of the SIF. First, for tensile loading in the zigzag direction, the crack is not straight. Bonds along the crack path are not parallel to the tensile loading direction, allowing more transverse displacements of atoms along the crack path than that for loading in the armchair direction. Second, at low value of the tensile force, the internal relaxation may play a larger role than that at high tensile force. Third, a relatively large initial crack length allows more internal relaxation due to a large number of initial broken bonds.

Effects of strain rate on the evolution of the SIF during crack propagation are shown in Figs. 11 and 12 for sheets pulled in the armchair and the zigzag directions, respectively. It is found that the critical SIF does not depend on strain rates for the range of strain rates examined in this work. For loading in the armchair direction at nominal axial strain rates of 2.5×10^6 and $2.5 \times 10^7 \text{ s}^{-1}$, the SIFs are essentially the same, and at the nominal axial strain rate of $2.5 \times 10^8 \text{ s}^{-1}$ the SIF also equals that for the other two strain rates during the early stages of crack propagation, and is slightly higher as the crack gets longer with the maximum difference in the SIF at strain rates of $2.5 \times 10^6 \text{ s}^{-1}$ and $2.5 \times 10^8 \text{ s}^{-1}$ equaling only $\sim 2\%$ at the final fracture stage; e.g., see Fig. 10-top for $a_0 = 3.5d$, $a_0/w = 0.022$.

For tensile loading in the zigzag direction, the SIFs are also unchanged for the three strain rates studied until the crack propagates to about 10% of the sheet's length in the direction perpendicular to the loading direction as shown in Fig. 12 for $a_0 = 5r$, $a_0/w = 0.018$. For longer cracks, due to crack branching shown in Fig. 8, the SIF fluctuates between 2.8 and 5.8 $\text{MPa}\sqrt{\text{m}}$ (3.4 and 4.5 $\text{MPa}\sqrt{\text{m}}$) at the strain rate of $2.5 \times 10^8 \text{ s}^{-1}$ ($2.5 \times 10^6 \text{ s}^{-1}$ and $2.5 \times 10^7 \text{ s}^{-1}$). Smooth segments of the SIF curves during crack

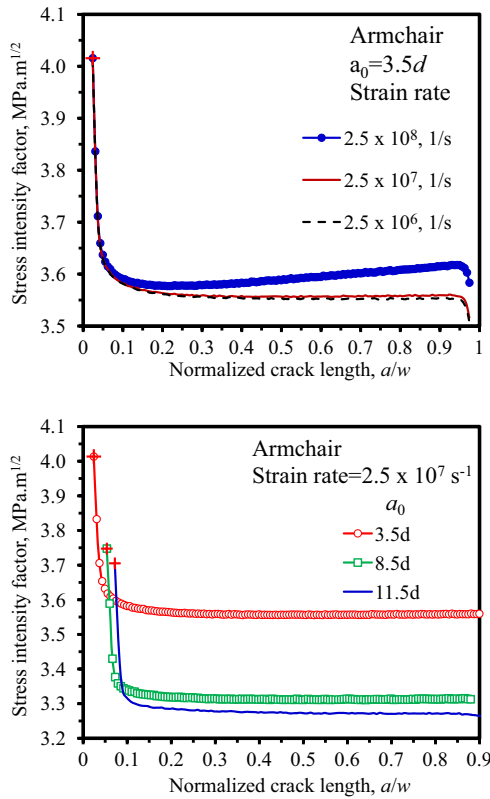


Fig. 11. Evolution of the stress intensity factor during crack propagation in graphene sheets under uniaxial tension in the armchair direction versus the normalized crack length, (top) effect of strain rates, (bottom) effect of initial crack length. The first point, marked by a red cross, in each curve corresponds to the critical stress intensity factor K_{Ic} . (For interpretation of the references to color in this figure legend, the reader is referred to the web version of this article.)

propagation marked by numbers 1,2,3... in Fig. 12 correspond to smooth shapes of the crack face also marked by numbers 1,2,3... in Fig. 8.

The effect of the initial crack length on the SIF is depicted in Fig. 11 (bottom) and Fig. 13. The critical SIF computed using Eq. (8) slightly decreases with an increase in the initial crack length for both armchair (variation is about 17% between the maximum and the minimum values) and zigzag (variation is about 5% between the maximum and the minimum values) directions. In contrast, using Eq. (9), the critical SIF is nearly constant for loading in the armchair direction, and slightly increases with an increase in the initial crack length for tension in the zigzag direction (variation is about 11% between the maximum and the minimum values). Differences in the critical SIFs computed by Eqs. (8) and (9) are about $\pm 8\%$. The mean values of the critical SIF and the standard deviation (DV) computed using Eqs. (8) and (9) along with results from the literature are listed in Table 3. The mean and the standard deviation values of the critical SIFs computed using Eq. (8) are $(3.8 \text{ MPa}\sqrt{\text{m}}, 0.17)$ and $(4.1 \text{ MPa}\sqrt{\text{m}}, 0.07)$ for the armchair and the zigzag directions, respectively; the corresponding values from Eq. (9) are $(4.0 \text{ MPa}\sqrt{\text{m}}, 0.03)$ and $(4.2 \text{ MPa}\sqrt{\text{m}}, 0.14)$. The SIF calculated using Eq. (8) becomes nearly independent of the initial crack length when it exceeds about 5% of the sheet width.

Our results for K_{Ic} agree well with those from a coupled QM/molecular mechanics study of Khare et al. [14] who found the critical SIF = $3.3\text{--}4.0 \text{ MPa}\sqrt{\text{m}}$ for an armchair monolayer graphene sheet, 3.71 (armchair) and $4.21 \text{ MPa}\sqrt{\text{m}}$ (zigzag) for a monolayer graphene computed by Xu et al. [9] using the QM/continuum mechanics approach, and Zhang et al.'s [11] experimental

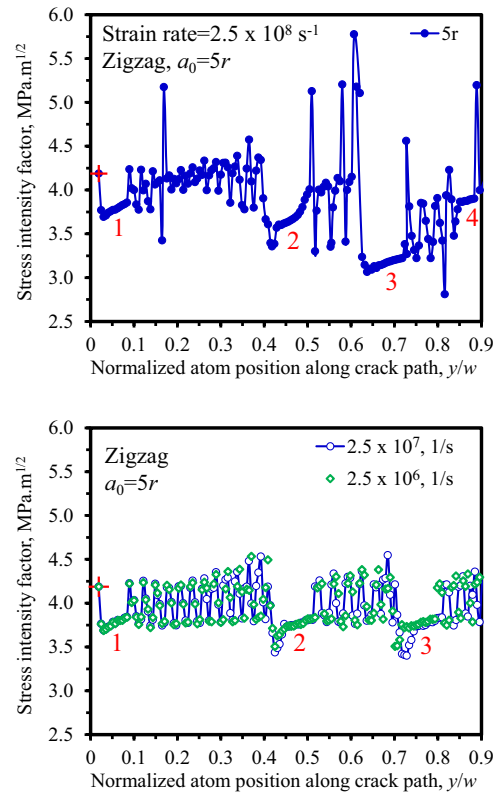


Fig. 12. Variation of the stress intensity factor during crack propagation in a zigzag graphene sheet with a single edge pre-crack of length $a_0 = 5r$ ($a_0/w = 0.018$) under uniaxial tension in the zigzag direction versus the normalized crack length at strain rate of (top) $2.5 \times 10^8 \text{ s}^{-1}$, and (bottom) $2.5 \times 10^7 \text{ s}^{-1}$ and $2.5 \times 10^6 \text{ s}^{-1}$. The first point (marked by a red cross) in each curve corresponds to the critical stress intensity factor K_{Ic} . Red numbers 1,2,3... indicates smooth segments of the SIF curves, which correspond to smooth shapes of the crack face; see also Fig. 8 and the text for details. (For interpretation of the references to color in this figure legend, the reader is referred to the web version of this article.)

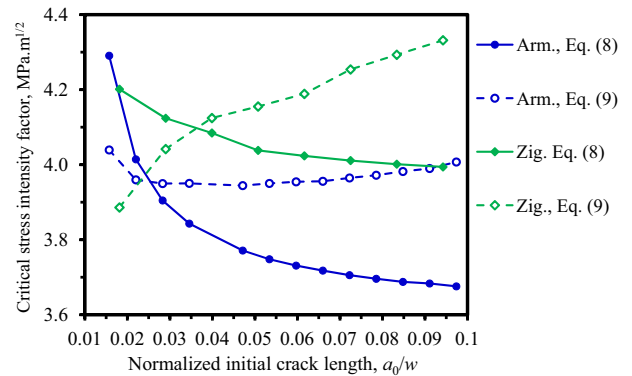


Fig. 13. Effects of the initial crack length on the critical stress intensity factor.

value of $4.0 \pm 0.6 \text{ MPa}\sqrt{\text{m}}$ for a monolayer, a bilayer, and a few-layered graphene sheet. We note that K_{Ic} was also found to be $10.7 \pm 3.3 \text{ MPa}\sqrt{\text{m}}$ for a SLGS [10], and $12.0 \pm 3.9 \text{ MPa}\sqrt{\text{m}}$ for a multilayer graphene sheet [38]. Samples used in experiments were polycrystalline graphene [10,11,38] while theoretical/computational studies have mostly simulated defect-free (except for a pre-crack) SLGSs. In a polycrystalline graphene sheet, the crack propagation direction changes as a crack propagates across a grain boundary [11]. The disordered layer stacking of multilayer graphene sheets also caused crack meandering [38] that was found

Table 3

Critical stress intensity factor K_{Ic} in $\text{MPa}\sqrt{\text{m}}$ (graphene sheet thickness t is assumed to be 3.4 Å for comparing present results with those in the literature, the abbreviation DV is used for standard deviation).

Reference	Fracture toughness ($\text{MPa}\sqrt{\text{m}}$)
Present study (average value), Eq. (8)	3.8 (armchair, DV = 0.17)
	4.1 (zigzag, DV = 0.07)
Present study (average value), Eq. (9)	4.0 (armchair, DV = 0.03)
	4.2 (zigzag, DV = 0.14)
Coupled QM/MM, Khare et al. [14]	3.3–4.0 (armchair)
Coupled QM/continuum mechanics, Xu et al. [9]	3.71 (armchair)
	4.21 (zigzag)
Experiments, Zhang et al. [11]	4.0 ± 0.6
Experiments, Hwangbo et al. [10]	10.7 ± 3.3
Experiments, Wei et al. [38]	12.0 ± 3.9

to increase the fracture toughness value to twice of the estimated value. Other main reasons for differences between the values from simulations and experiments may be crack blunting [11] and crack branching [10,38]. Compared with the atomically sharp crack-tip, the blunt notch reduces the local stress concentration, leading to an increase in the far-field fracture stress [11]. Crack branching could multiply the crack length by several times when the crack follows a complex path, and could significantly increase the fracture toughness of the monolayer and the multilayered graphene sheets [10,38].

5. Conclusions

We have studied through MD simulations and the Tersoff potential the fracture of an edge-cracked single layer graphene sheet. Main findings are summarized below.

- A simple method based on the crack-tip stress field is proposed to compute the SIF during crack propagation in a nano-structure.
- During the early stages of crack propagation, the computed critical SIF is essentially the same for strain rates of $2.5 \times 10^6 \text{ s}^{-1}$, $2.5 \times 10^7 \text{ s}^{-1}$ and $2.5 \times 10^8 \text{ s}^{-1}$. For the first two values of the axial strain rate, the SIFs during crack propagation are almost identical under tensile loading in the armchair direction, and different for tensile loading in the zigzag direction. For loading in the armchair direction, the SIF at a strain rate of $2.5 \times 10^8 \text{ s}^{-1}$ is slightly higher than that at the other two strain rates when the crack has noticeably elongated.
- For tensile loading in the zigzag direction, the SIF fluctuates due to crack branching, the corresponding crack faces are not smooth, and these fluctuations increase with an increase in the applied strain rate. The SIF varies between 2.8 and $5.8 \text{ MPa}\sqrt{\text{m}}$ for the strain rate of $2.5 \times 10^8 \text{ s}^{-1}$, and between 3.4 and $4.5 \text{ MPa}\sqrt{\text{m}}$ for the other two strain rates.
- The critical SIF computed with the crack-tip stress field differs by about $\pm 8\%$ from that found using the global axial stress.

Using the crack-tip stress field, the SIF varied with the initial crack length by about 17% and 5% for tensile loading in the armchair and the zigzag directions, respectively. However, when the global axial stress is used to compute the SIF, it is essentially independent of the initial crack length for loading in the armchair direction, and vary by about 11% for loading in the zigzag direction. The mean values of the critical SIF are 3.8 (armchair) and $4.1 \text{ MPa}\sqrt{\text{m}}$ (zigzag) from the crack-tip stress field, and 4.0 (armchair) and $4.2 \text{ MPa}\sqrt{\text{m}}$ (zigzag) from the average stress field. These values agree well with the literature theoretical [9,14] and experimental [11] results.

Acknowledgements

Minh-Quy Le's work was supported by the Vietnam National Foundation for Science and Technology Development (NAFOSTED) grant 107.02-2014.03. R.C. Batra's work was partially funded by the US ONR grant N00014-11-1-0594 with Dr. Y.D.S. Rajapakse as the Program Manager.

References

- [1] C. Lee et al., *Science* 321 (2008) 385–388.
- [2] A.A. Balandin et al., *Nano Lett.* 8 (3) (2008) 902–907.
- [3] K. Bolotin et al., *Solid State Commun.* 146 (9–10) (2008) 351–355.
- [4] D. Li, R.B. Kaner, *Science* 320 (2008) 1170–1171.
- [5] S. Stankovich et al., *Nature* 442 (2006) 282–286.
- [6] Y. Jin, F.G. Yuan, *J. Nanosci. Nanotechnol.* 5 (4) (2005) 601–608.
- [7] Z. Zhang, X. Wang, J.D. Lee, *J. Appl. Phys.* 115 (2014) 114314.
- [8] G.S. Jung, Z. Qin, M.J. Buehler, *Extreme Mech. Lett.* 2 (2015) 52–59.
- [9] M. Xu et al., *Int. J. Fract.* 173 (2012) 163–173.
- [10] Y. Hwangbo et al., *Sci. Rep.* 4 (2014) 4439.
- [11] P. Zhang et al., *Nat. Commun.* 5 (2014) 3782.
- [12] D. Datta et al., *Extreme Mech. Lett.* 5 (2015) 10–17.
- [13] K. Nakatani, Y. Sugiyama, H. Kitagawa, *AIAA J.* 38 (4) (2000) 695–701.
- [14] R. Khare et al., *Phys. Rev. B* 75 (2007).
- [15] Y. Jin, F.G. Yuan, *J. Nanosci. Nanotechnol.* 5 (12) (2005) 2099–2107.
- [16] M.Q. Le, R.C. Batra, *Comput. Mater. Sci.* 84 (2014) 238–243.
- [17] M.Q. Le, R.C. Batra, *Comput. Mater. Sci.* 69 (2013) 381–388.
- [18] J. Tersoff, *Phys. Rev. B* 39 (8) (1989) 5566–5568.
- [19] L. Lindsay, D.A. Broido, *Phys. Rev. B* 81 (2010) 205441.
- [20] T. Belytschko et al., *Phys. Rev. B* 65 (2002).
- [21] O.A. Shenderova et al., *Phys. Rev. B* 61 (2000).
- [22] M. Sammalakorpi et al., *Phys. Rev. B* 70 (2004).
- [23] B.W. Jeong, J.K. Lim, S.B. Sinnotta, *Appl. Phys. Lett.* 90 (2007).
- [24] H.U. Jäger, K. Albe, *J. Appl. Phys.* 88 (2000) 1129.
- [25] M. Huhtala et al., *Phys. Rev. B* 70 (2004) 045404.
- [26] D.W. Brenner et al., *J. Phys.: Condens. Matter* 14 (2002) 783–802.
- [27] D. Troya, S.L. Mielke, G.C. Schatz, *Chem. Phys. Lett.* 382 (2003) 133–141.
- [28] S. Zhang et al., *Phys. Rev. B* 71 (2005) 115403.
- [29] S. Plimpton, *J. Comput. Phys.* 117 (1) (1995) 1–19.
- [30] T. Schneider, E. Stoll, *Phys. Rev. B* 17 (1978) 1302.
- [31] S.S. Gupta, R.C. Batra, *J. Comput. Theor. Nanosci.* 7 (10) (2010) 2151–2164.
- [32] R.C. Batra, S.S. Gupta, *J. Appl. Mech. – Trans. ASME.* 75 (6) (2008) 061010.
- [33] G. Marc, W.G. McMillan, *Adv. Chem. Phys.* 58 (1985) 209.
- [34] J.A. Zimmerman et al., *Modell. Simul. Mater. Sci. Eng.* 12 (2004) S319–S332.
- [35] F. Liu, P. Ming, J. Li, *Phys. Rev. B* 76 (2007) 064120.
- [36] M. Xu et al., *Int. J. Solids Struct.* 49 (18) (2012) 2582–2589.
- [37] T.L. Anderson, *Fracture Mechanics: Fundamentals and Applications*, third ed., CRC Press, Taylor, Francis Group, 2005.
- [38] X. Wei et al., *Nano Lett.* 15 (2015) 689–694.